Volume 53
Number 47
21 December 2024
Pages 18793-19008

Dalton Transactions

An international journal of inorganic chemistry

rsc.li/dalton

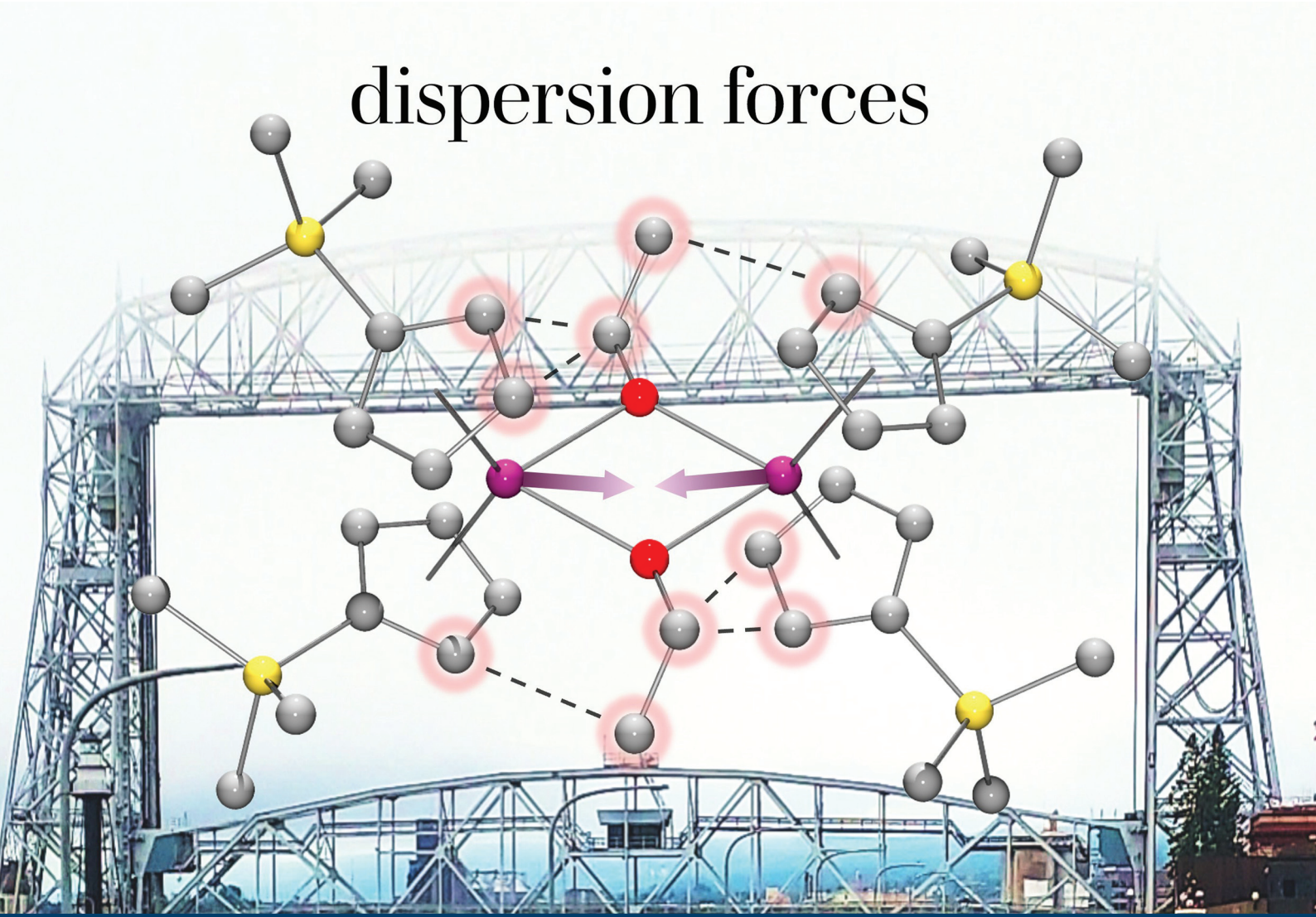

Themed issue: New Talent Americas

ISSN 1477-9226

ROYAL SOCIETY OF CHEMISTRY

PAPER

Daniel N. Huh *et al.*

Synthesis and reduction of $[(C_5H_4SiMe_3)_2Ln(\mu\text{-}OR)]_2$ (Ln = La, Ce) complexes: structural effects of bridging alkoxides

Dalton Transactions

ROYAL SOCIETY OF CHEMISTRY

PAPER

View Article Online
View Journal | View Issue

Cite this: *Dalton Trans.*, 2024, **53**, 18856

Synthesis and reduction of $[(C_5H_4SiMe_3)_2Ln(\mu\text{-}OR)]_2$ (Ln = La, Ce) complexes: structural effects of bridging alkoxides†

Adrian N. Brown, [a] Jack N. Kelleher, [a] Alexander M. Brown, [b] Peter Saghy, [b] Joshua J. Bohl, [a] Jerome R. Robinson *[b] and Daniel N. Huh *[a]

Received 24th July 2024,
Accepted 19th August 2024

DOI: 10.1039/d4dt02137a

rsc.li/dalton

Alcoholysis of Cp'_3Ln (Ln = La, Ce; Cp′ = $C_5H_4SiMe_3$) generate high-yielding (72–97%) bimetallic Ln^{III} complexes of $[Cp'_2Ln(\mu\text{-}OR)]_2$ [R = Et, ^{i}Pr, or C_6H_4-4-^{t}Bu]. Single-crystal X-ray diffraction of these complexes reveal unexpected decreases in Ln···Ln distances, increasing Cp_{cent}–Ln–Cp_{cent} angles, and increasing intermolecular C···C contacts with bulkier bridging alkoxides, in line with structural control driven by significant dispersion forces. ^{1}H NMR spectroscopy of $[Cp'_2Ce(\mu\text{-}OEt)]_2$ and $[Cp'_2Ce(\mu\text{-}O^iPr)]_2$ revealed significantly upfield resonances assigned as methylene and methine moieties of −43.74 and −70.85 ppm, respectively. 2D ^{1}H DOSY NMR experiments of $[Cp'_2Ce(\mu\text{-}O^iPr)]_2$ in C_6D_6 supported a dimeric structure in solution, including in the presence of a Lewis base (*i.e.*, THF). Reduction of $[Cp'_2La(\mu\text{-}O^iPr)]_2$ using KC_8 in the presence of 2.2.2-cryptand at −78 °C generated a purple solution and X-band EPR spectroscopy revealed an eight-line hyperfine pattern indicative of a La^{II} species.

Introduction

Bimetallic lanthanide (Ln) complexes have served as useful compounds for polymerization catalysis[1–3] as well as research areas including single-molecular magnetism (SMM) and quantum information science (QIS).[4–14] Reduction chemistry of bimetallic Ln complexes has recently emerged as a method to form mixed-valent Ln^{III}/Ln^{II} species,[15,16] with intervalence-charge transfer (IVCT) character (*i.e.* Robin-Day Class II or III categorization) and in some cases, yielding Ln–Ln bonds with large coercive magnetic fields.[10] Reductive Ln chemistry has typically been examined for monometallic compounds. Low-valent Ln ions supported by cyclopentadienide derivatives, for example, have been shown to have interesting physical properties/performance including reinforced magnetic phase memory,[17–20] and molecular qudit properties.[21] Recently, there have also been several reports involving syntheses of hetero-multimetallic complexes including Ln/Al (Ln = Sm, Dy, Y, Yb) supported by tris(pyrazolyl)borates,[22] Ln/V (Ln = La, Nd, Gd, Yb, Er) with bridging redox-active ligands,[23] Y/M (M = Al, Ga) containing C_5Me_5 and a boryl moiety,[24] Ln_2/Al_2 (Ln = La, Nd) isoprene polymerization catalyst,[25] Ce_2/Cu alkoxide complex,[26] and Ln/Ni (Ln = Y, La, Lu) complexes supported by a crown-ether-like macrocycle.[27]

Synthesis of homobimetallic complexes supported by cyclopentadienyl ligands and bridged by alkoxides or aryloxides, $[Cp^R_2Ln(\mu\text{-}OR)]_2$, in particular, have historically been reported *via* two synthetic routes: (1) reductive cleavage of glycols,[28–30] and (2) alcoholysis[31–35] (Fig. 1). Due to their small steric profile compared to amido or cyclopentadienyl groups, alkoxide and aryloxides can frequently promote formation of bimetallic species. Of the reported $[Cp^R_2Ln(\mu\text{-}OR)]_2$ complexes, only two La[29,32] and four Ce[28,31,32] have been published. Often these compounds are presented as side-products from reduction reactions in the presence of glycols or as an additional means to synthesize heteroleptic Cp/alkoxide compounds. However, assessing the structural impact of the bridging alkoxide moiety is often overlooked and revisiting this class of compounds could provide useful insights to subtle structural modulations.

Herein, we report the synthesis of $[Cp'_2Ln(\mu\text{-}OR)]_2$ (Cp′ = $C_5H_4SiMe_3$; Ln = La, Ce; R = Et, ^{i}Pr, C_6H_4-4-^{t}Bu) complexes *via* alcoholysis of Cp'_3Ln generating yields of 72–97%. 2D ^{1}H DOSY NMR and SC-XRD unambiguously identify the dimer structure of these complexes. Structural analyses reveal unexpected decreases in Ln···Ln distances, increases in Cp_{cent}–Ln–Cp_{cent} angles, and increases in intermolecular C···C contacts with bulkier bridging alkoxides, in line with structural control

[a]*Department of Chemistry, University of Rhode Island, Kingston, RI 02881, USA. E-mail: danhuh@uri.edu*
[b]*Department of Chemistry, Brown University, Providence, RI 02912, USA. E-mail: jerome_robinson@brown.edu*

†Electronic supplementary information (ESI) available. CCDC 2372725–2372727. For ESI and crystallographic data in CIF or other electronic format see DOI: https://doi.org/10.1039/d4dt02137a

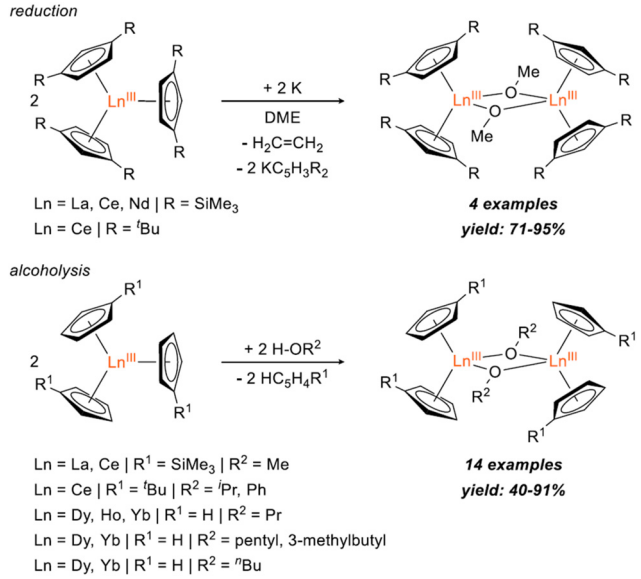

Fig. 1 Reported syntheses of $[Cp^R{}_2Ln(\mu\text{-}OR)]_2$ bimetallic complexes *via* reduction[28,29] (top) and alcoholysis[31–35] (bottom).

driven by significant dispersion forces. Finally, reduction of $[Cp'_2La(\mu\text{-}O^iPr)]_2$ using KC_8 in the presence of 2.2.2-cryptand generated a transient La^{II} species characterized by CW X-band EPR.

Results and discussion

Alcoholysis reactions of Cp'_3Ln (**1-Ln**, Ln = La, Ce) using HO-R (R = Et, ^{i}Pr, C_6H_4-4-^{t}Bu) in Et_2O at room temperature form isolable bimetallic complexes $[Cp'_2Ln(\mu\text{-}OR)]_2$ **2-Ln/R** in 72–97% yields (Fig. 2). Evans' method of **2-Ce/R** have magnetic

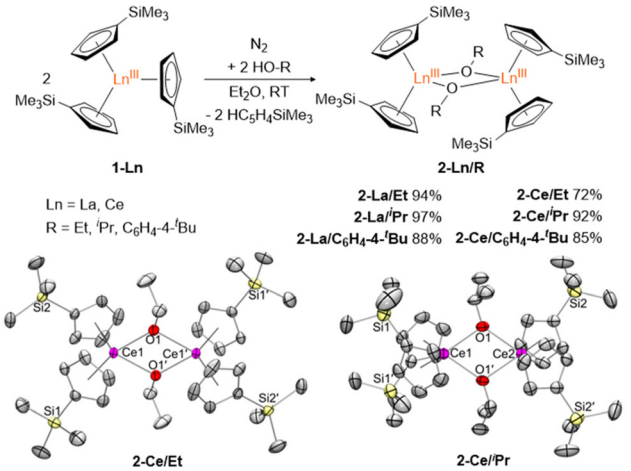

Fig. 2 Top: synthesis of **2-Ln/R** by alcoholysis of **1-Ln** in Et_2O. Bottom: crystal structures of **2-Ce/Et** and **2-Ce/^{i}Pr** with displacement ellipsoids at the 50% probability level. Hydrogen atoms and disorder were removed for clarity.

moments of 1.28 (R = Et), 1.90 (R = ^{i}Pr), and 1.34μ_B (R = C_6H_4-4-^{t}Bu) (Fig. S12–S15†). UV-vis data (Fig. S16†) of **2-Ce/R** in toluene were also collected and have λ_{max} values of 458 (R = Et), 452 (R = ^{i}Pr), and 471 nm (R = C_6H_4-4-^{t}Bu). These values are similar to the reported UV-vis spectrum of **2-Ce/Me** in toluene with a λ_{max} of 475 nm.[32] Crystals suitable for SC-XRD were structurally characterized for $[Cp'_2Ce(\mu\text{-}OEt)]_2$ **2-Ce/Et**, $[Cp'_2La(\mu\text{-}O^iPr)]_2$ **2-La/^{i}Pr**, and $[Cp'_2Ce(\mu\text{-}O^iPr)]_2$ **2-Ce/^{i}Pr**. Despite numerous attempts, X-ray quality single crystals of $[Cp'_2Ln(\mu\text{-}OC_6H_4\text{-}4\text{-}^tBu)]_2$ (**2-Ln/C_6H_4-4-^{t}Bu**, Ln = La and Ce) were unable to be obtained.

The metrical parameters of **2-La/^{i}Pr**, **2-Ce/Et**, and **2-Ce/^{i}Pr** are summarized in Table 1. Crystallographic data of 14 structures adopting the $[Cp_2Ln(\mu\text{-}OR)]_2$ (R = alkyl) geometry have been reported.[28–35] Of these compounds, only two La complexes and three Ce complexes were reported: $[Cp'_2La(\mu\text{-}OMe)]_2$,[32] $\{[C_5H_3(SiMe_3)_2]_2La(\mu\text{-}OMe)\}_2$,[29] $[Cp'_2Ce(\mu\text{-}OMe)]_2$,[32] $[(C_5H_4{}^tBu)_2Ce(\mu\text{-}O^iPr)]_2$,[31] and $[(C_5H_3{}^tBu_2)_2Ce(\mu\text{-}OMe)]_2$[28] (Table 1). Despite the increased steric bulk offered by the isopropyl group, Ln···Ln distances of **2-Ln/^{i}Pr** are significantly shorter than that of the reported **2-Ln/Me**; [La: 3.8119(4) and 3.8428(4) *vs.* 3.8566(4) Å; Ce: 3.7977(8) and 3.7810(8) *vs.* 3.8286(6) Å].[32] Upon closer inspection of the **2-Ln/^{i}Pr** and **2-Ce/Et** complexes, several short intramolecular C···C distances ($d_{C\cdots C}$) are present between the R groups (^{i}Pr, Et) and sp^2 carbons of the Cp′ ligand, approaching 3.644(3) and 3.641(3) Å, respectively (Fig. S1†). These distances are much shorter than the *tert*-butyl-substituted trityl compound, $[C(C_6H_3\text{-}3,5\text{-}^tBu_2)_3]_2$, which is well-established to display significant dispersion forces [$d_{C\cdots C}$: 3.95(2)–4.15(2) Å].[36–39] Furthermore, the Cp_{cent}–Ln–Cp_{cent} angles of **2-Ce/Et**, **2-La/^{i}Pr**, and **2-Ce/^{i}Pr** range from 129.69 to 132.92° (Table 1), which are the largest angles observed for any $[Cp^R{}_2Ln(\mu\text{-}OR)]$ architecture (123.9 to 128.9°).[28,31–35,40,41] Taken together, the observed distortions for **2-Ce/Et**, **2-La/^{i}Pr**, and **2-Ce/^{i}Pr** (*i.e.*, shorter than expected Ln···Ln distances and larger Cp_{cent}–Ln–Cp_{cent} angles) are likely stabilized *via* significant inter-ligand dispersion forces.

All hydrogen signals of **2-Ln/R** complexes were identifiable at RT using ^{1}H NMR spectroscopy (Fig. 3). **2-Ln/R** displayed effective D_{2h} symmetry in solution, with the anticipated number of peaks present R = Et (5), ^{i}Pr (5), C_6H_4-4-^{t}Bu (6). For the paramagnetic Ce^{III} complexes, these resonances spanned a relatively large range covering ~+20 to −70 ppm. Notably, methylene and methine hydrogens of **2-Ce/Et** and **2-Ce/^{i}Pr**, respectively, were observed at significantly negative shifts: OCH_2Me, −43.74 and OCHMe$_2$, −70.85 ppm. Other Ce^{III} alkoxides have been reported along with their partial ^{1}H NMR assignment, *e.g.*, $[(C_5H_4{}^tBu)_2Ce^{III}(\mu\text{-}O^iPr)]_2$[31] $[(^tBuCHO)_2Ce^{III}(\mu\text{-}OCH^tBu)]_2$,[42] $[C_5H_3{}^tBu_2]_2Ce^{III}(OC_6H_{11})(THF)$, however, this marks the first observation of Ce^{III} alkoxide –CH resonances by ^{1}H NMR spectroscopy.

Given the resolution and relatively long t_1 relaxation time,[43–45] ^{1}H DOSY NMR data was collected to establish whether the dimeric nature of **2-Ce/^{i}Pr** in the solid-state was conserved in solution (Fig. 4). 2D ^{1}H DOSY NMR experiments provided a diffusion coefficient used to calculate an effective

Table 1 Selected bond distances (Å) and angles (°) for $[Cp'_2La(\mu\text{-}O^iPr)]_2$ (**2-La/^{i}Pr**) $[Cp'_2Ce(\mu\text{-}OEt)]_2$ (**2-Ce/Et**), $[Cp'_2Ce(\mu\text{-}O^iPr)]_2$ (**2-Ce/^{i}Pr**) and previously reported $[Cp_2Ln(\mu\text{-}OR)]_2$ structures

	2-La/Me[32]	**2-La/^{i}Pr**	**2-Ce/Me**[32]	**2-Ce/Et**	**2-Ce/^{i}Pr**	$[(C_5H_3{}^tBu_2)_2Ce(\mu\text{-}OMe)]_2$[28]	$[(C_5H_4{}^tBu)_2Ce(\mu\text{-}O^iPr)]_2$[31]
Ln–O	2.375(1), 2.413(1)	2.360(1), 2.364(1), 2.377(1), 2.403(1)	2.350(3), 2.387(2)	2.335(1), 2.360(1)	2.339(4), 2.339(4), 2.347(4), 2.361(4)	2.366(3), 2.386(4)	2.369(3), 2.373(3)
Ln–Cp_{cent}	2.562, 2.572	2.572, 2.573, 2.578, 2.581	2.531, 2.539	2.532, 2.551	2.541, 2.542, 2.542, 2.546	2.564, 2.596	2.565, 2.577
Ln···Ln	3.8566(4)	3.8119(4), 3.8428(4)	3.8286(6)	3.8052(6)	3.7977(8), 3.7810(8)	3.887(1)	3.844(2)
Ln–O–Ln	107.31(4)	107.02(4), 107.56(5)	107.85(9)	108.28(4)	107.59(2), 107.78(1)	109.8(1)	108.3(1)
Cp_{cent}–Ln–Cp_{cent}	128.22	130.42, 130.5, 131.33, 132.92	127.67	131.38	129.69, 129.96, 130.13, 130.17	126.20	128.51
Shortest C···C[a]	3.546(2)	3.645(3)	3.521(2)	3.563(3)	3.64(2)	3.74(1)	3.67(1)
sp^2 C···C < 4.0 Å[b]	4	17	4	10	17	2	18

[a] Shortest intramolecular C···C distance between a cyclopentadienide and –OR group. [b] Number of intramolecular C···C distances less than 4.0 Å between sp^2 cyclopentadienide and –OR.

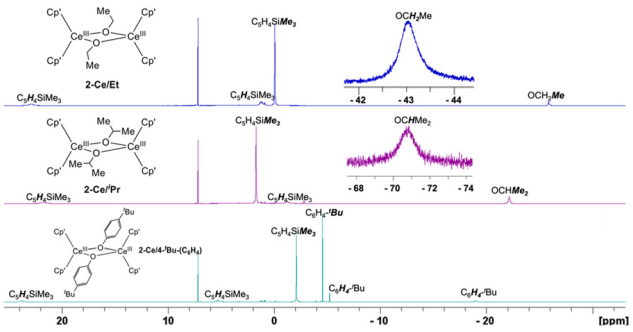

Fig. 3 ^{1}H NMR 298 K spectra in C_6D_6 of **2-Ce/Et**, **2-Ce/^{i}Pr**, and **2-Ce/C_6H_4-^{t}Bu** including insets of significantly upfield methylene and methine ^{1}H signals of **2-Ce/Et** and **2-Ce/^{i}Pr**, respectively.

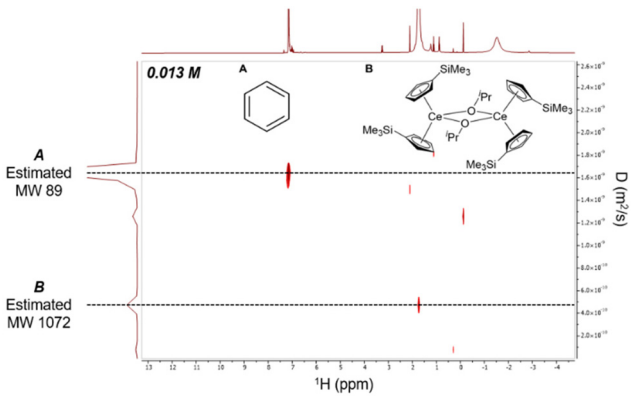

Fig. 4 2D ^{1}H DOSY NMR spectra of 0.013 M **2-Ce/^{i}Pr** in C_6D_6 demonstrating preservation of dimer in solution.

molecular weight of 1072 g mol^{-1} *via* the Stokes–Einstein Gierer–Wirtz Estimation (SEGWE) model[46,47] and a hydrodynamic radius (r_H) of 7.0 Å using the Stokes–Einstein equation.[48,49] These were in good agreement with the expected molecular weight (948 g mol^{-1}) and r_H from the crystal structure (7.4 Å, Fig. S20†), in line with a dimeric structure of **2-Ce/^{i}Pr** in C_6D_6. Furthermore, ^{1}H NMR of **2-Ce/^{i}Pr** in the presence of 2 equiv. of THF maintained an effective molecular weight of 1152 g mol^{-1} and r_H of 7.4 Å, suggesting that the dimeric structure was also maintained in the presence of moderate-strength Lewis bases (Fig. S11 and S15†).

Electrochemistry of 2-Ln/^{i}Pr

With a comprehensive understanding of the solution-structures of **2-Ln/R**, we evaluated the electrochemical behavior of **2-Ln/^{i}Pr** using cyclic voltammetry (CV) and differential pulse voltammetry (DPV). CVs and DPVs of **2-La/^{i}Pr** (~2.5 mM) in THF using 100 mM $[NBu_4][PF_6]$ collected from +0.5 to −3.5 V *vs.* Fc revealed two irreversible features. Starting at ~−0.25 V, an irreversible reduction was observed around −3.3 V scanning cathodically, while an irreversible oxidation was observed with an onset of ~0.2 V. These were tentatively assigned as an irreversible $La^{III/II}$ reduction and ligand oxidation, respectively.

CVs and DPVs of **2-Ce/^{i}Pr** revealed a similar irreversible reduction (E_{pc} = −3.32 V), along with three irreversible oxidations (E_{pa} = −0.20, −0.07, and +0.28 V). The oxidative event at +0.28 V generated a corresponding reductive feature at −1.25 V, which may be associated with the $Ce^{III/IV}$ couple (see ESI†). Notably, Evans and coworkers reported irreversible reductions for Cp'_3La^{III} and Cp'_3Ce in THF around the same potential (−3.36 and −3.43 V *vs.* Fc),[50] which suggest a relatively minor impact of ligand identity (Cp′ *vs.* O^{i}Pr) and nuclearity (monomer *vs.* dimer) on the electrochemical accessibility of the non-classical ($4f^n5d^1$) La^{II} and Ce^{II} ions. While evaluation of additional compounds would be needed to fully validate this observation, our results clearly indicate accessible reductive and oxidative events within the bimetallic **2-Ln/^{i}Pr** complexes.

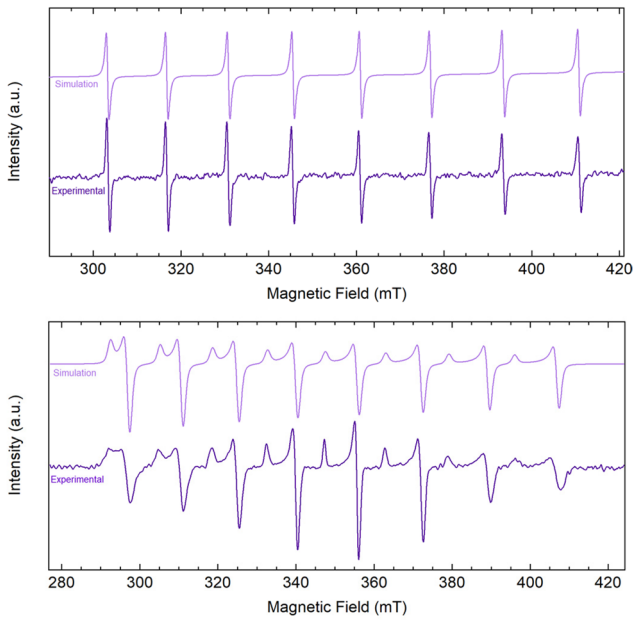

Fig. 5 *EasySpin*[52] simulation and experimental CW X-band EPR spectra of the reduction of $[Cp'_2La(\mu\text{-}O^{i}Pr)]_2$ (**2-La/^{i}Pr**) with KC_8 and 2.2.2-cryptand dissolved in THF (~5 mM) collected at 298 K (mode: perpendicular; g_{ave} = 1.970; A_{ave} = 424 MHz (153 G); ν = 9.856 GHz) (top) and at 77 K (mode: perpendicular $g_{\parallel}$ = 2.005, $g_{\perp}$ = 1.963; $A_{\parallel}$ = 417 MHz (149 G), $A_{\perp}$ = 431 MHz (157 G); ν = 9.653 GHz) (bottom).

Reduction of 2-La/^{i}Pr

Encouraged by the electrochemical behavior of **2-Ln/^{i}Pr**, chemical reduction of **2-La/^{i}Pr** was pursued. Addition of KC_8 and 2.2.2-cryptand to THF solutions of **2-La/^{i}Pr** at −78 °C immediately generated purple-colored mixtures. After removing graphite *via* filtration at −78 °C, a thermally-sensitive purple solution was obtained. The reduction product generated from **2-La/^{i}Pr** + KC_8 + 2.2.2-cryptand was significantly more sensitive than $[Cp'_3La^{II}]^{1-}$ reported by Evans and coworkers, where the reduction of Cp'_3La^{III} was possible at room temperature.[51] Upon warming to room temperature, the solution undergoes decomposition to an intractable yellow oil within 30 min. Attempts to remove solvent under reduced pressure or recrystallization at −35 °C also yielded intractable yellow oils. Alternatively, purple solutions of the reduction product were much more stable at −78 °C, where no decomposition was observed over the course of 4 h. The improved stability under these conditions enabled additional characterization by X-band EPR spectroscopy at 77 K and 298 K prior to decomposition (Fig. 5). At room temperature, the reduction product exhibited an isotropic, 8-line EPR spectrum [g_{ave} = 1.970 and A_{ave} = 424 MHz (153 G)], due to clear hyperfine coup-

Table 2 Summary of reported La^{II} EPR *g*-values, A-values (MHz and G) at various temperatures

La^{II} species	*T* (K)	*g*	*A* (MHz)	*A* (G)	Ref.
$[Cp'_3La]^{1-}$	80 295	$g_{\parallel}$ = 1.999 $g_{\perp}$ = 1.956 g_{ave} = 1.994	$A_{\parallel}$ = 420 $A_{\perp}$ = 430 A_{ave} = 430	$A_{\parallel}$ = 150 $A_{\perp}$ = 157 A_{ave} = 154	51
$\{[C_5H_3(SiMe_3)_2]_3La\}^{1-}$	80 298	$g_{\parallel}$ = 2.001 $g_{\perp}$ = 1.950 g_{ave} = 1.97	$A_{\parallel}$ = 392 $A_{\perp}$ = 385 A_{ave} = 366.2	$A_{\parallel}$ = 140 $A_{\perp}$ = 141 A_{ave} = 133.7	53–55
$\{[C_5H_4{}^{t}Bu]_3La\}^{1-}$	77 298	$g_{\parallel}$ = 1.995 $g_{\perp}$ = 1.941 g_{ave} = 1.959	— —	$A_{\parallel}$ = 197 $A_{\perp}$ = 208 A_{ave} = 204 G	56
$\{[C_5H_3{}^{t}Bu_2]_3La\}^{1-}$	40	$g_{\parallel}$ = 1.998 $g_{\perp}$ = 1.934	$A_{\parallel}$ = 650 $A_{\perp}$ = 630	$A_{\parallel}$ = 232 $A_{\perp}$ = 233	57
$[(C_5H_4Me)_3La]^{1-}$	298	g_{ave} = 1.971	—	A_{ave} = 195	58
$[(C_5Me_4H)_3La]^{1-}$	298	g_{ave} = 1.970	A_{ave} = 802	A_{ave} = 291	59
This work	77 298	$g_{\parallel}$ = 2.005 $g_{\perp}$ = 1.963 g_{ave} = 1.970	$A_{\parallel}$ = 417 $A_{\perp}$ = 431 A_{ave} = 424	$A_{\parallel}$ = 149 $A_{\perp}$ = 157 A_{ave} = 153	[a]

[a] This work

ling with the ^{139}La nucleus (I = 7/2). Alternatively, at 77 K, the reduction product exhibited an axial, 16-line EPR spectrum [$g_{\|}$ = 2.005, $g_{\perp}$ = 1.963; $A_{\|}$ = 417 MHz (149 G), $A_{\perp}$ = 431 MHz (157 G)]. Both spectra were consistent with the formation of a La^{II} species and were readily modelled using EasySpin.[52] Although the A-value parameters are similar to $[Cp'_3La]^{1-}$, the g-values are distinct and only a single La^{II} species was observed (Table 2). These observations are inconsistent with ligand redistribution of **2-La/^{i}Pr** + KC_8 to form $[Cp'_3La]^{1-}$. Other examples of ligand redistribution after reduction of mixed ligand systems, however, have resulted in significant speciation.[29,53] Additionally, UV-vis spectra of the reduction were collected (Fig. S17†) with absorption features located at 563, 859, and 938 nm.

These absorbances are different than the reported [K(2.2.2-cryptand)][Cp'_3La^{II}] of 554 nm.[51] Taken together, the initial chemical reduction studies are consistent with the accessible reductive events observed by CV and DPV, and further investigation of the reductive and oxidative reactivity of **2-Ln/R** and other bimetallic Ln are promising areas for future studies.

Conclusions

We have synthesized several new Ln metallocenes bridged by alkoxide or aryloxide *via* alcoholysis in good to excellent yields and characterized them by NMR and SC-XRD. X-ray crystal structures of **2-Ln/^{i}Pr** and **2-Ce/Et** reveal decreasing Ln···Ln distances, increasing Cp_{cent}–Ln–Cp_{cent} angles, and increasing intermolecular C···C contacts with bulkier bridging alkoxides. These suggest that significant dispersion forces mediated by the R groups (R = Et, ^{i}Pr) could control the structure of the [Ln(μ-OR)]$_2$ core. All hydrogens in **2-Ce/R** complexes were identified using ^{1}H NMR including methylene (R = Et) and methine (R = ^{i}Pr) hydrogens which were observed as highly upfield signals. 2D ^{1}H DOSY NMR confirmed that the dimeric structure of **2-Ce/^{i}Pr** in the solid-state was maintained in solution, while electrochemical studies of **2-Ln/^{i}Pr** suggested accessible reductive and oxidative events. Chemical reduction of **2-La/^{i}Pr** using KC_8 in the presence of 2.2.2-cryptand at −78 °C generated a purple solution and EPR spectroscopy supported the formation of a novel La^{II} species. Our studies indicate that heteroleptic cyclopentadienide/alkoxide systems readily support the formation of bimetallic complexes in the solid- and solution-state with accessible redox events. Further investigations of constructing bimetallic f element complexes containing non-covalent interactions and reduction chemistry to determine their ability to form mixed-valent and/or metal–metal bonds are ongoing.

Experimental

General considerations

All synthesis techniques described below were conducted under nitrogen with exclusion of air using glovebox and Schlenk-line techniques. KC_8,[60] $Ln[C_5H_4SiMe_3]_3$[51] (Ln = La, Ce), and $KC_5H_4SiMe_3$[61] were prepared using previously published procedures. Hexanes, toluene, THF, and Et_2O were dried using a pure process technology solvent purification system and stored over activated 4 Å molecular sieves. EtOH and ^{i}PrOH were degassed with three freeze-pump-thaw cycles and stored over activated 4 Å molecular sieves. HOC_6H_4-4-^{t}Bu was degassed under vacuum overnight and prior to use. NMR solvent C_6D_6 was dried using NaK, degassed with three freeze-pump-thaw cycles, and vacuum-transferred prior to use. ^{1}H, ^{13}C NMR and Evans' method data were obtained on a Bruker Avance III 300 MHz or Bruker AvanceHD 400 MHz spectrometer at 298 K (see ESI for spectra). UV-vis data were collected on a Shimadzu UV-3600 Plus using a sealed 5 mm quartz cuvette (see ESI spectra). Elemental analysis was data collected through the Center for Enabling New Technologies Through Catalysis (CENTC) at the University Rochester using a PerkinElmer 2400 Series II Analyzer.

Synthesis of [Cp′$_2$La(μ-OEt)]$_2$ (2-La/Et)

In an N_2-filled glovebox, EtOH (21 μL, 0.36 mmol) was added into a transparent Et_2O (10 mL) solution of Cp'_3La (**1-La**) (199 mg, 0.36 mmol), yielding an opaque, colorless mixture. The mixture was allowed to stir for 2 h, after which volatiles (HCp′ and Et_2O) were removed *in vacuo* to yield a microcrystalline colorless solid (159 mg, 94%). ^{1}H (400 MHz, C_6D_6, 25 °C, δ, ppm): 6.69 (t, 8H, $C_5\boldsymbol{H_4}SiMe_3$), 6.42 (t, 8H, $C_5\boldsymbol{H_4}SiMe_3$), 3.32 (q, 4H, OC$\boldsymbol{H_2}CH_3$), 1.16 (t, 6H, $OCH_2C\boldsymbol{H_3}$), 0.39 (s, 36H, $C_5H_4Si\boldsymbol{Me_3}$). $^{13}C\{^1H\}$ (100.6 MHz, C_6D_6, 25 °C, δ, ppm): 124.09 ($\boldsymbol{C_5}H_4SiMe_3$), 121.36 ($\boldsymbol{C_5}H_4SiMe_3$), 117.91 ($\boldsymbol{C_5}H_4SiMe_3$), 59.69 (O$\boldsymbol{C}H_2$Me), 21.13 ($OCH_2\boldsymbol{Me}$), 0.78 ($C_5H_4Si\boldsymbol{Me_3}$). Anal. calcd for $C_{36}H_{62}O_2Si_4La_2{\cdot}OEt_2$: C, 48.47; H, 7.32. Found: C, 48.76; H, 7.19.

Synthesis of [Cp′$_2$La(μ-O^{i}Pr)]$_2$ (2-La/^{i}Pr)

As described for **2-La/Et**, ^{i}PrOH (36 μL, 0.45 mmol) was added to a colorless Et_2O (10 mL) solution of Cp'_3La (**1-La**) (251 mg, 0.45 mmol) and colorless solids were isolated (208 mg, 97%). Single crystal X-ray quality crystals were obtained from a concentrated Et_2O solution at −35 °C. ^{1}H (400 MHz, C_6D_6, 25 °C, δ, ppm): 6.73 (t, 8H, $C_5\boldsymbol{H_4}SiMe_3$), 6.40 (t, 8H, $C_5\boldsymbol{H_4}SiMe_3$), 3.13 (m, 2H, OC$\boldsymbol{H}Me_2$), 1.25 (d, 12H, OCH$\boldsymbol{Me_2}$), 0.43 (s, 36H, $C_5H_4Si\boldsymbol{Me_3}$). $^{13}C\{^1H\}$ (100.6 MHz, C_6D_6, 25 °C, δ, ppm): 123.23 ($\boldsymbol{C_5}H_4SiMe_3$), 122.02 ($\boldsymbol{C_5}H_4SiMe_3$), 117.59 ($\boldsymbol{C_5}H_4SiMe_3$), 64.70 (O$\boldsymbol{C}HMe_2$), 27.98 (OCH$\boldsymbol{Me_2}$), 1.08 ($C_5H_4Si\boldsymbol{Me_3}$). Anal. calcd for $C_{38}H_{66}O_2Si_4La_2$: C, 48.29; H, 7.04. Found: C, 48.51; H, 7.20.

Synthesis of [Cp′$_2$La(μ-OC$_6$H$_4$-4-^{t}Bu)]$_2$ (2-La/OC$_6$H$_4$-4-^{t}Bu)

In a N_2-filled glovebox, Et_2O (10 mL) was added to a combination of Cp'_3La (212 mg, 0.38 mmol) and 4-*tert*-butylphenol (57 mg, 0.38 mmol), which yielded a colorless opaque solution seconds after stirring was initiated. The solution stirred for 24 h, after which the solvent was removed *in vacuo* to yield a colorless powder (191 mg, 88%). ^{1}H (400 MHz, C_6D_6, 25 °C, δ, ppm): 7.25 (d, 4H, $OC_6\boldsymbol{H_4}$-4-^{t}Bu), 6.93 (d, 4H, $OC_6\boldsymbol{H_4}$-4-^{t}Bu), 6.73 (s, 8H, $C_5\boldsymbol{H_4}SiMe_3$), 6.65 (s, 8H, $C_5\boldsymbol{H_4}SiMe_3$), 1.36 (s, 18H, OC_6H_4-4-$^t\boldsymbol{Bu}$). 0.101 (s, 36H, $C_5H_4Si\boldsymbol{Me_3}$). $^{13}C\{^1H\}$ (100.6 MHz, C_6D_6, 25 °C, δ, ppm): 153.69 ($O\boldsymbol{C_6}H_4$-4-^{t}Bu), 144.47 ($O\boldsymbol{C_6}H_4$-4-^{t}Bu), 128.11

(O***C***$_6$H$_4$-4-^{t}Bu), 124.89 (***C***$_5$H$_4$SiMe$_3$), 123.34 (***C***$_5$H$_4$SiMe$_3$), 119.50 (O***C***$_6$H$_4$-4-^{t}Bu), 118.60 (***C***$_5$H$_4$SiMe$_3$), 34.29 (OC$_6$H$_4$-4-^{t}***Bu***), 31.66 (OC$_6$H$_4$-4-^{t}***Bu***), 0.20 (C$_5$H$_4$Si***Me***$_3$). Anal. calcd for $C_{52}H_{78}O_2Si_4La_2$: C, 55.50; H, 6.99. Found: C, 55.61; H, 6.91.

Synthesis of [Cp′$_2$Ce(μ-OEt)]$_2$ (2-Ce/Et)

In an N_2-filled glovebox, EtOH (16 μL, 0.26 mmol) was syringed into a royal blue Et_2O (10 mL) solution of Cp′$_3$Ce (146 mg, 0.26 mmol), immediately yielding a transparent, golden-yellow solution. The solution was stirred for 30 min and volatiles (HCp′ and Et_2O) were removed *in vacuo* to yield a golden-yellow solid (133.8 mg, 72%). Single crystal X-ray quality yellow crystals were obtained after storing a concentrated hexanes solution at −35 °C in a freezer overnight. ^{1}H (400 MHz, C_6D_6, 25 °C, δ, ppm): 23.12 (s, 8H, C$_5$***H***$_4$SiMe$_3$), 0.97 (s, 8H, C$_5$***H***$_4$SiMe$_3$), −0.05 (s, 36H, C$_5$H$_4$Si***Me***$_3$), −26.24 (s, 6H, OCH$_2$C***H***$_3$), −43.74 (s, 4H, OC***H***$_2$CH$_3$). Evans method: 1.28μ_B. UV-vis (THF) λ_{max}, nm (ε, M^{-1} cm^{-1}): 458 (555). Anal. calcd for $C_{36}H_{62}O_2Si_4Ce_2{\cdot}0.5OEt_2$: C, 47.72; H, 7.06. Found: C, 47.67; H, 6.71.

Synthesis of [Cp′$_2$Ce(μ-O^{i}Pr)]$_2$ (2-Ce/^{i}Pr)

As described for **2-Ce/Et**, ^{i}PrOH (48 μL, 0.63 mmol) was added into a royal blue Et_2O (10 mL) solution of Cp′$_3$Ce (346 mg, 0.63 mmol) and a bright yellow solid was isolated (274.3 mg, 92%). Single crystal X-ray quality crystals were obtained from a concentrated hexanes solution after storing in a −35 °C freezer overnight. ^{1}H (300 MHz, C_6D_6, 25 °C, δ, ppm): 21.75 (s, 8H, C$_5$***H***$_4$SiMe$_3$), 1.69 (s, 36H, C$_5$H$_4$Si***Me***$_3$), −1.25 (s, 8H, C$_5$***H***$_4$SiMe$_3$), −22.16 (s, 12H, OCH***Me***$_2$), −70.85 (s, 2H, OC***H***Me$_2$). Evans method: 1.90μ_B. UV-vis (THF) λ_{max}, nm (ε, M^{-1} cm^{-1}): 452 (650). Anal. calcd for $C_{38}H_{66}O_2Si_4Ce_2$: C, 48.17; H, 7.02. Found: C, 48.49; H, 6.94.

Synthesis of [Cp′$_2$Ce(μ-OC$_6$H$_4$-4-^{t}Bu)]$_2$ (2-Ce/OC$_6$H$_4$-4-^{t}Bu)

In an N_2-filled glovebox, a diethyl ether (5 mL) solution of HOC$_6$H$_4$-4-^{t}Bu (14 mg, 0.091 mmol) was added to a royal blue Et_2O (5 mL) solution of Cp′$_3$Ce (50 mg, 0.091 mmol), yielding a dark yellow solution after 15 seconds of stirring. The solution was allowed to stir for 30 minutes, after which the product was dried *in vacuo* to yield a dark yellow solid (80.7 mg, 85%). ^{1}H (300 MHz, C_6D_6, 25 °C, δ, ppm): 23.73 (s, 8H, C$_5$***H***$_4$SiMe$_3$), 5.26 (s, 8H, C$_5$***H***$_4$SiMe$_3$), −2.10 (s, 36H, C$_5$H$_4$Si***Me***$_3$), −4.57 (s, 18H, OC$_6$H$_4$-4-^{t}***Bu***), −5.23 (s, 4H, OC$_6$***H***$_4$-4-^{t}Bu), −18.98 (s, 4H, OC$_6$***H***$_4$-4-^{t}Bu). Evans method: 1.34μ_B. UV-vis (THF) λ_{max}, nm (ε, M^{-1} cm^{-1}): 471 (731). Anal. calcd for $C_{52}H_{78}O_2Si_4Ce_2$: C, 55.38; H, 6.97. Found: C, 55.57; H, 6.94.

Reduction of 2-La/^{i}Pr

In a N_2-filled glovebox, THF (10 mL) solution of **2-La/^{i}Pr** (50 mg, 0.053 mmol) and a flask containing KC_8 (8 mg, 0.059 mmol) and 2.2.2-cryptand (22 mg, 0.059 mmol) were chilled in a −78 °C coldwell for 1 h. The **2-La/^{i}Pr** THF solution was added to the KC_8 and 2.2.2-cryptand mixture and swirled vigorously for 5 min. A purple-solution with graphite immediately formed. While in the coldwell, the purple mixture was filtered through a dry Celite plug to remove graphite yielding a purple solution. UV-vis (THF) λ_{max}, nm: 563, 859, 938.

X-ray crystallography

Samples were removed from their mother liquor in an inert-atmosphere glovebox, covered in Paraton™ oil in a separate 20 mL vial, sealed with electrical tape and stored within a sealed jar, and transported to Brown University. These samples were transferred to a glass slide where it was evaluated and mounted with the assistance of an optical microscope. X-ray reflection intensity data were collected on a Bruker D8 Venture with a Photon III CPAD detector employing a IμS 3.0 Mo-Kα radiation source (λ = 0.71073 Å) at a temperature of 173(1) K. Rotation frames were integrated using SAINT,[62] producing a listing of unaveraged F^2 and $\sigma(F^2)$ values which were then passed to the SHELXT[63] program package for further processing and structure solution. The intensity data were corrected for Lorentz and polarization effects and for absorption using SADABS.[64] The structures were solved by using SHELXT,[63] using Olex2 as the graphical interface.[65] Refinement was by full-matrix least squares based on F^2 using SHELXL.[66] All reflections were used during refinements. Non-hydrogen atoms were refined anisotropically and hydrogen atoms were refined using a riding model. Disorders were refined with the help of similarity restraints using standard/default values on 1,2 and 1,3 distances (SADI) and rigid bond restraints (RIGU) of the disordered groups.[67,68]

EPR spectroscopy

EPR spectra were collected on a Bruker EMX Premium-X spectrometer with a field strength of 9.65 GHz and a microwave power of 2.0 mW at 77 K using a liquid-nitrogen finger dewar (Wilmad, 50 mL Suprasil). Sample solutions (~5 mM) were prepared as nitrogen-saturated, toluene solutions in 4 mm o.d. quartz EPR tubes. Samples were glassed by slowly lowering the sample into liquid nitrogen (~2 mm s^{-1}). The experimental spectra were simulated using *EasySpin*.[52] In all cases, a representative fit was achieved through the use of the Nelder/Mead simplex model algorithm while assuming isotropic line broadening.

Electrochemistry

All electrochemistry experiments were conducted using a CH Instruments (CHI) 700E series potentiostat and performed under inert atmosphere in a nitrogen-filled glovebox outfitted with electrical leads (KF-40 port). The electrochemical cells consisted of 4 mL vials using THF as solvent with 100 mM [NBu_4][PF_6] as the electrolyte, 1–5 mM analyte (**2-Ce/^{i}Pr** or **2-La/^{i}Pr**), a glassy carbon electrode (3 mm, CHI) as the working electrode, a platinum wire as the counter electrode, and a Ag/Ag^+ non-aqueous electrode (CHI, THF, 100 mM [NBu_4][PF_6],10 mM AgOTf) as the reference electrode. The working electrode was polished to a shiny-mirror like finish with 0.05 micron micropolish powder (CH Instruments) and washed with water and acetone outside of the glovebox, brought inside the glovebox, and inserted into the electrochemical cell. The working electrode was replaced periodically

upon scanning irreversible oxidation or reduction features to prevent fouling of the electrode surface. All data were collected in a positive-feedback IR compensation mode; cell resistances measured with THF as a solvent were 150–250 Ω. Differential pulse voltammetry experiments (DPV) were performed using the same electrochemical cell and electrodes, as well as the same IR compensation procedure. All DPVs were collected at 10 mV s^{-1}, with a 30 s quiet time before each scan.

Author contributions

Adrian N. Brown: conceptualization, investigation, formal analysis, writing – original draft, writing – review & editing. Jack N. Kelleher: investigation, formal analysis, writing – original draft, writing – review & editing. Alexander M. Brown: investigation, formal analysis. Peter Saghy: investigation, formal analysis. Joshua J. Bohl: investigation. Jerome R. Robinson: investigation, formal analysis, writing – original draft, writing – review & editing. Daniel N. Huh: conceptualization, writing – review & editing, supervision, funding acquisition.

Data availability

Crystallographic data for **2-Ce/Et**, **2-La/^{i}Pr**, and **2-Ce/^{i}Pr** have been deposited at the CCDC under 2372725, 2372726, and 2372727, respectively and can be obtained from ccdc.cam.ac.uk/structures.†

Conflicts of interest

There are no conflicts to declare.

Acknowledgements

Financial support for this research was provided by the University of Rhode Island (DNH: start-up funds) and the National Science Foundation (EPR and electrochemistry accessories purchased from CHE-1900248). Instrumentation for the University of Rhode Island Chemistry 400 MHz AvanceHD was supported from a grant through the National Science Foundation (CHE-1531963). X-ray diffraction experiments were performed with a diffractometer purchased through a grant through the NSF-MRI program (CHE-2117549) located at Brown University. Elemental analysis data was collected by the CENTC at the University of Rochester (CHE-0650456).

References

1 J. Qin, B. Xu, Y. Zhang, D. Yuan and Y. Yao, Cooperative rare earth metal–zinc based heterometallic catalysts for copolymerization of CO_2 and cyclohexene oxide, *Green Chem.*, 2016, **18**, 4270–4275.

2 Q. Yao, Y. Wang, B. Zhao, X. Zhu, Y. Luo, D. Yuan and Y. Yao, Syntheses of Heterometallic Neodymium–Zinc Complexes and Their Performance in the Copolymerization of CO_2 and Cyclohexene Oxide, *Inorg. Chem.*, 2022, **61**, 10373–10382.

3 K. Yin, L. Hua, L. Qu, Q. Yao, Y. Wang, D. Yuan, H. You and Y. Yao, Heterobimetallic rare earth metal–zinc catalysts for reactions of epoxides and CO_2 under ambient conditions, *Dalton Trans.*, 2021, **50**, 1453–1464.

4 F. Delano IV, F. Benner, S. Jang and S. Demir, Pyrrolyl-Bridged Metallocene Complexes: From Synthesis, Electronic Structure, to Single-Molecule Magnetism, *Inorg. Chem.*, 2023, **62**, 14604–14614.

5 C. A. Gould, E. Mu, V. Vieru, L. E. Darago, K. Chakarawet, M. I. Gonzalez, S. Demir and J. R. Long, Substituent Effects on Exchange Coupling and Magnetic Relaxation in 2,2′-Bipyrimidine Radical-Bridged Dilanthanide Complexes, *J. Am. Chem. Soc.*, 2020, **142**, 21197–21209.

6 F. Benner and S. Demir, From unprecedented 2,2′-bisimidazole-bridged rare earth organometallics to magnetic hysteresis in the dysprosium congener, *Inorg. Chem. Front.*, 2023, **10**, 4981–4992.

7 F. Benner, L. La Droitte, O. Cador, B. Le Guennic and S. Demir, Magnetic hysteresis and large coercivity in bis-benzimidazole radical-bridged dilanthanide complexes, *Chem. Sci.*, 2023, **14**, 5577–5592.

8 P. Zhang, R. Nabi, J. K. Staab, N. F. Chilton and S. Demir, Taming Super-Reduced Bi_2^{3-} Radicals with Rare Earth Cations, *J. Am. Chem. Soc.*, 2023, **145**, 9152–9163.

9 F. Benner and S. Demir, Isolation of the elusive bisbenzimidazole $Bbim^{3-\bullet}$ radical anion and its employment in a metal complex, *Chem. Sci.*, 2022, **13**, 5818–5829.

10 C. A. Gould, K. R. McClain, D. Reta, J. G. C. Kragskow, D. A. Marchiori, E. Lachman, E. Choi, J. G. Analytis, R. D. Britt, N. F. Chilton, B. G. Harvey and J. R. Long, Ultrahard magnetism from mixed-valence dilanthanide complexes with metal-metal bonding, *Science*, 2022, **375**, 198–202.

11 H. Kwon, K. R. McClain, J. G. C. Kragskow, J. K. Staab, M. Ozerov, K. R. Meihaus, B. G. Harvey, E. S. Choi, N. F. Chilton and J. R. Long, Coercive Fields Exceeding 30 T in the Mixed-Valence Single-Molecule Magnet $(Cp^{iPr5})_2Ho_2I_3$, *J. Am. Chem. Soc.*, 2024, **146**, 18714–18721.

12 C. Uhlmann, L. Münzfeld, A. Hauser, T. Ruan, S. K. Kuppusamy, C. Jin, M. Ruben, K. Fink, E. Moreno-Pineda and P. W. Roesky, Unique Double and Triple Decker Arrangements of Rare-Earth 9,10-Diborataanthracene Complexes Featuring Single-Molecule Magnet Characteristics, *Angew. Chem., Int. Ed.*, 2024, **63**, e202401372.

13 J. Long, F. Habib, P. Lin, I. Korobkov, G. Enright, L. Ungur, W. Wernsdorfer, L. F. Chibotaru and M. Murugesu, Single-Molecule Magnet Behavior for an Antiferromagnetically Superexchange-Coupled Dinuclear Dysprosium(III) Complex, *J. Am. Chem. Soc.*, 2011, **133**, 5319–5328.

14 P. Lin, T. Burchell, R. Clérac and M. Murugesu, Dinuclear Dysprosium(III) Single-Molecule Magnets with a Large Anisotropic Barrier, *Angew. Chem., Int. Ed.*, 2008, **47**, 8848–8851.

15 J. C. Wedal, L. Anderson-Sanchez, M. T. Dumas, C. A. Gould, M. J. Beltrán-Leiva, C. Celis-Barros, D. Páez-Hernández, J. W. Ziller, J. R. Long and W. J. Evans, Synthesis and Crystallographic Characterization of a Reduced Bimetallic Yttrium ansa-Metallocene Hydride Complex, [K(crypt)][(μ-Cp^{An})Y(μ-H)]$_2$ (Cp^{An} = Me$_2$Si[C$_5$H$_3$(SiMe$_3$)-3]$_2$), with a 3.4 Å Yttrium–Yttrium Distance, *J. Am. Chem. Soc.*, 2023, **145**, 10730–10742.

16 M. D. Roy, T. P. Gompa, S. M. Greer, N. Jiang, L. S. Nassar, A. Steiner, J. Bacsa, B. W. Stein and H. S. La Pierre, Intervalence, Charge Transfer in Nonbonding, Mixed-Valence, Homobimetallic Ytterbium Complexes, *J. Am. Chem. Soc.*, 2024, **146**, 5560–5568.

17 C. A. P. Goodwin, F. Ortu, D. Reta, N. F. Chilton and D. P. Mills, Molecular magnetic hysteresis at 60 kelvin in dysprosocenium, *Nature*, 2017, **548**, 439–442.

18 C. A. Gould, K. R. McClain, J. M. Yu, T. J. Groshens, F. Furche, B. G. Harvey and J. R. Long, Synthesis and Magnetism of Neutral, Linear Metallocene Complexes of Terbium(II) and Dysprosium(II), *J. Am. Chem. Soc.*, 2019, **141**, 12967–12973.

19 K. R. McClain, C. A. Gould, D. A. Marchiori, H. Kwon, T. T. Nguyen, K. E. Rosenkoetter, D. Kuzmina, F. Tuna, R. D. Britt, J. R. Long and B. G. Harvey, Divalent Lanthanide Metallocene Complexes with a Linear Coordination Geometry and Pronounced 6s–5d Orbital Mixing, *J. Am. Chem. Soc.*, 2022, **144**, 22193–22201.

20 A. Ariciu, D. H. Woen, D. N. Huh, L. E. Nodaraki, A. K. Kostopoulos, C. A. P. Goodwin, N. F. Chilton, E. J. L. McInnes, R. E. P. Winpenny, W. J. Evans and F. Tuna, Engineering electronic structure to prolong relaxation times in molecular qubits by minimising orbital angular momentum, *Nat. Commun.*, 2019, **10**, 3330.

21 L. E. Nodaraki, A. M. Ariciu and D. N. Huh, Ligand Effects on the Spin Relaxation Dynamics and Coherent Manipulation of Organometallic La(II), Potential Qudits, *J. Am. Chem. Soc.*, 2024, **146**, 15000–15009.

22 T. Chowdhury, F. Murphy, A. R. Kennedy, C. Wilson, J. H. Farnaby and C. E. Weetman, Synthesis and Reactivity of Bis-tris(pyrazolyl)borate Lanthanide/Aluminum Heterobimetallic Trihydride Complexes, *Inorg. Chem.*, 2024, **63**, 9390–9394.

23 J. R. Hickson, S. J. Horsewill, C. Bamforth, J. McGuire, C. Wilson, S. Sproules and J. H. Farnaby, The modular synthesis of rare earth-transition metal heterobimetallic complexes utilizing a redox-active ligand, *Dalton Trans.*, 2018, **47**, 10692–10701.

24 M. Bonath, D. Schädle, C. Maichle-Mössmer and R. Anwander, The Alkylaluminate/Gallate Trap: Metalation of Benzene by Heterobimetallic Yttrocene Complexes [Cp*$_2$Y(MMe$_3$R)] (M = Al, Ga), *Inorg. Chem.*, 2021, **60**, 14952–14968.

25 E. C. Moinet, P. Wetzel, O. Tardif, C. Maichle-Mössmer and R. Anwander, Ancillary Ligand-Free Mixed Chlorido/Isobutylaluminato Lanthanide Complexes in Isoprene Polymerization, *Organometallics*, 2024, **43**, 611–616.

26 H. Tsurugi, Y. Ikeda, K. Shinohara, S. Shirase, N. Toya, S. Tanaka and K. Mashima, Synthesis and Characterization of Alkoxide-Bridged Heterometallic Clusters of Cerium and Copper, *Inorg. Chem.*, 2019, **58**, 12565–12572.

27 J. P. Karnes, A. Kumar, J. A. Hopkins Leseberg, V. W. Day and J. D. Blakemore, Trivalent Cations Slow Electron Transfer to Macrocyclic Heterobimetallic Complexes, *Inorg. Chem.*, 2024, **63**, 8710–8729.

28 Y. K. Gun'ko, P. B. Hitchcock and M. F. Lappert, Activation of a C-O bond by reaction of a tris(cyclopentadienyl)lanthanide complex with an alkali metal in dimethoxyethane (DME); crystal structures of [Ndη-C$_5$H$_3$(SiMe$_3$)$_2$-1,3$_2$(μ-OMe)$_2$Li(DME)] and [{Ce(η-C$_5$H$_3$^{t}Bu$_2$-1,3)$_2$(μ-OMe)$_2$], *J. Organomet. Chem.*, 1995, **499**, 213–219.

29 M. C. Cassani, M. F. Lappert and F. Laschi, First identification by EPR spectra of lanthanum(II) organometallic intermediates (and $E^1_{\frac{1}{2}}$ for La^{3+} → La^{2+}) in the C–O bond activation of dimethoxyethane, *Chem. Commun.*, 1997, 1563–1564.

30 A. V. Khvostov, V. K. Belsky, B. M. Bulychev, A. I. Sizov and B. B. Ustinov, *ansa*-Ytterbocenes(+3) with a short bridge and bulky substituents: synthesis and crystal structure of *meso*-(CH$_3$)$_2$Si[3-(CH$_3$)$_3$SiC$_5$H$_3$]$_2$YbCl(THF), *rac*-(CH$_3$)$_2$C[3-^{t}BuC$_5$H$_3$]$_2$Yb(μ^2-Cl)$_2$Li(OEt$_2$)$_2$, and [*meso*-(CH$_3$)$_2$C[3-^{t}BuC$_5$H$_3$]$_2$Yb(μ^2-OCH$_3$)]$_2$, *J. Organomet. Chem.*, 1998, **571**, 243–249.

31 S. D. Stults, R. A. Andersen and A. Zalkin, Chemistry of trivalent cerium and uranium metallocenes: reactions with alcohols and thiols, *Organometallics*, 1990, **9**, 1623–1629.

32 C. T. Palumbo, L. E. Darago, C. J. Windorff, J. W. Ziller and W. J. Evans, Trimethylsilyl versus Bis(trimethylsilyl) Substitution in Tris(cyclopentadienyl) Complexes of La, Ce, and Pr: Comparison of Structure, Magnetic Properties, and Reactivity, *Organometallics*, 2018, **37**, 900–905.

33 Z. Wu, Z. Xu, X. You, X. Zhou and Z. Jin, Synthesis and characterization of binuclear organolanthanide complexes involving cyclopentadienyl and n-propyloxide ligands. X-ray crystal structure of [(C$_5$H$_5$)$_2$Yb(μ-OCH$_2$CH$_2$CH$_3$)]$_2$, *Polyhedron*, 1992, **11**, 2673–2678.

34 Z. Wu, Z. Huang, R. Cai, Z. Xu, X. You and X. Huang, Synthesis and characterization of dinuclear organolanthanide alkoxides, X-ray crystal structures of [(C$_5$H$_5$)$_2$Yb(μ-OCH$_2$CH$_2$CH$_2$CH$_2$CH$_3$)]$_2$ and [(C$_5$H$_5$)Yb(μ-OCH$_2$CH$_2$CH(Me)$_2$]$_2$, *Polyhedron*, 1996, **15**, 13–22.

35 W. Zhongzhi, X. Zheng, Y. Xiaozeng, Z. Xigeng and H. Xiaoying, Dehydrogenation of organolanthanide alkoxides and X-ray crystal structures of the reaction product [{(C$_5$H$_5$)$_2$Ln(μ-O(Me)C-CHCH$_3$)}$_2$] (Ln = Dy Yb), *J. Organomet. Chem.*, 1994, **483**, 107–113.

36 E. Osawa, Y. Onuki and K. Mislow, The central bond length in hexaphenylethane and hexakis(2,6-di-tert-butyl-4-biphenylyl)ethane, *J. Am. Chem. Soc.*, 1981, **103**, 7475–7479.

37 W. D. Hounshell, D. A. Dougherty, J. P. Hummel and K. Mislow, Structure of hexaphenylethane and congeners as determined by empirical force field calculations, *J. Am. Chem. Soc.*, 1977, **99**, 1916–1924.

38 S. Grimme and P. R. Schreiner, Steric Crowding Can Stabilize a Labile Molecule: Solving the

Hexaphenylethane Riddle, *Angew. Chem., Int. Ed.*, 2011, **50**, 12639–12642.
39 D. Liptrot and P. Power, London dispersion forces in sterically crowded inorganic and organometallic molecules, *Nat. Rev. Chem.*, 2017, **1**, 0004.
40 S. Pagano and W. Schnick, Di-μ-tert-butanolato-bis[bis(η^5-cyclopentadienyl)erbium(III)], *Acta Crystallogr., Sect. E: Struct. Rep. Online*, 2008, **64**, m473.
41 Y. Luo, Y. Yao, Q. Shen and Y. Xing, Synthesis and Crystal Structure of Bis(tert-butyl-cyclopentadienyl) Erbium Ethoxide,(t-BuCp)$_2$ErOEt, *J. Rare Earths*, 2002, **20**, 374.
42 H. A. Stecher, A. Sen and A. L. Rheingold, Synthesis, structure, and reactivity of cerium(III) alkoxides. 2. Thermal decomposition of Ce(OC-tert-Bu$_3$)$_3$ and the structure of [Ce(OCH-tert-Bu$_2$)$_3$]$_2$, *Inorg. Chem.*, 1989, **28**, 3280–3282.
43 M. P. Crockett, H. Zhang, C. M. Thomas and J. A. Byers, Adding diffusion ordered NMR spectroscopy (DOSY) to the arsenal for characterizing paramagnetic complexes, *Chem. Commun.*, 2019, **55**, 14426–14429.
44 J. R. Robinson, Z. Gordon, C. H. Booth, P. J. Carroll, P. J. Walsh and E. J. Schelter, Tuning Reactivity and Electronic Properties through Ligand Reorganization within a Cerium Heterobimetallic Framework, *J. Am. Chem. Soc.*, 2013, **135**, 19016–19024.
45 J. R. Robinson, Y. Qiao, J. Gu, P. J. Carroll, P. J. Walsh and E. J. Schelter, The role of dynamic ligand exchange in the oxidation chemistry of cerium(III), *Chem. Sci.*, 2016, **7**, 4537–4547.
46 R. Evans, G. Dal Poggetto, M. Nilsson and G. A. Morris, Improving the Interpretation of Small Molecule Diffusion Coefficients, *Anal. Chem.*, 2018, **90**, 3987–3994.
47 R. Evans, Z. Deng, A. K. Rogerson, A. S. McLachlan, J. J. Richards, M. Nilsson and G. A. Morris, Quantitative Interpretation of Diffusion-Ordered NMR Spectra: Can We Rationalize Small Molecule Diffusion Coefficients?, *Angew. Chem., Int. Ed.*, 2013, **52**, 3199–3202.
48 E. J. Cabrita and S. Berger, DOSY studies of hydrogen bond association: tetramethylsilane as a reference compound for diffusion studies, *Magn. Reson. Chem.*, 2001, **39**, S142–S148.
49 D. Li, G. Kagan, R. Hopson and P. G. Williard, Formula Weight Prediction by Internal Reference Diffusion-Ordered NMR Spectroscopy (DOSY), *J. Am. Chem. Soc.*, 2009, **131**, 5627–5634.
50 M. T. Trinh, J. C. Wedal and W. J. Evans, Evaluating electrochemical accessibility of 4f^{n}5d^1 and 4f^{n+1} Ln(ii) ions in (C$_5$H$_4$SiMe$_3$)$_3$Ln and (C$_5$Me$_4$H)$_3$Ln complexes, *Dalton Trans.*, 2021, **50**, 14384–14389.
51 M. E. Fieser, M. R. MacDonald, B. T. Krull, J. E. Bates, J. W. Ziller, F. Furche and W. J. Evans, Structural, Spectroscopic, and Theoretical Comparison of Traditional vs Recently Discovered Ln2+ Ions in the [K(2.2.2-cryptand)][(C$_5$H$_4$SiMe$_3$)$_3$Ln] Complexes: The Variable Nature of Dy^{2+} and Nd^{2+}, *J. Am. Chem. Soc.*, 2015, **137**, 369–382.
52 S. Stoll and A. Schweiger, EasySpin, a comprehensive software package for spectral simulation and analysis in EPR, *J. Magn. Reson.*, 2006, **178**, 42–55.
53 S. A. Moehring and W. J. Evans, Evaluating Electron-Transfer Reactivity of Complexes of Actinides in +2 and +3 Oxidation States by using EPR Spectroscopy, *Chem. – Eur. J.*, 2020, **26**, 1530–1534.
54 D. N. Huh, J. W. Ziller and W. J. Evans, Chelate-Free Synthesis of the U(II) Complex, [(C$_5$H$_3$(SiMe$_3$)$_2$)$_3$U]$^{1-}$, Using Li and Cs Reductants and Comparative Studies of La(II) and Ce(II) Analogs, *Inorg. Chem.*, 2018, **57**, 11809–11814.
55 P. Hitchcock, M. Lappert, L. Maron and A. Protchenko, Lanthanum Does Form Stable Molecular Compounds in the +2 Oxidation State, *Angew. Chem., Int. Ed.*, 2008, **47**, 1488–1491.
56 M. A. Angadol, D. H. Woen, C. J. Windorff, J. W. Ziller and W. J. Evans, tert-Butyl(cyclopentadienyl) Ligands Will Stabilize Nontraditional +2 Rare-Earth Metal Ions, *Organometallics*, 2019, **38**, 1151–1158.
57 J. Liu, L. E. Nodaraki, D. O. T. A. Martins, M. J. Giansiracusa, P. J. Cobb, J. Emerson-King, F. Ortu, G. F. S. Whitehead, G. K. Gransbury, E. J. L. McInnes, F. Tuna and D. P. Mills, Non-classical early lanthanide(II) di-tert- butylcyclopentadienyl complexes, *Eur. J. Inorg. Chem.*, 2023, **26**, e202300552.
58 D. H. Woen, D. N. Huh, J. W. Ziller and W. J. Evans, Reactivity of Ln(II) Complexes Supported by (C$_5$H$_4$Me)1− Ligands with THF and PhSiH3: Isolation of Ring-Opened, Bridging Alkoxyalkyl, Hydride, and Silyl Products, *Organometallics*, 2018, **37**, 3055–3063.
59 T. F. Jenkins, D. H. Woen, L. N. Mohanam, J. W. Ziller, F. Furche and W. J. Evans, Tetramethylcyclopentadienyl Ligands Allow Isolation of Ln(II) Ions across the Lanthanide Series in [K(2.2.2-cryptand)][(C$_5$Me$_4$H)$_3$Ln] Complexes, *Organometallics*, 2018, **37**, 3863–3873.
60 D. E. Bergbreiter and J. M. Killough, Reactions of potassium-graphite, *J. Am. Chem. Soc.*, 1978, **100**, 2126–2134.
61 J. K. Peterson, M. R. MacDonald, J. W. Ziller and W. J. Evans, Synthetic Aspects of (C$_5$H$_4$SiMe$_3$)$_3$Ln Rare-Earth Chemistry: Formation of (C$_5$H$_4$SiMe$_3$)$_3$Lu via [(C$_5$H$_4$SiMe$_3$)$_2$Ln]$^+$ Metallocene Precursors, *Organometallics*, 2013, **32**, 2625–2631.
62 *Bruker SAINT, v8.37a*, Bruker AXS Inc., Madison, Wisconsin, 2012.
63 G. M. Sheldrick, SHELXT–Integrated space-group and crystal-structure determination, *Acta Crystallogr., Sect. A: Found. Adv.*, 2015, **71**, 3–8.
64 *Bruker SADABS, v2014/5*, Bruker AXS Inc., Madison, Wisconsin, 2001.
65 O. V. Dolomanov, L. J. Bourhis, R. J. Gildea, J. A. Howard and H. Puschmann, OLEX2: a complete structure solution, refinement and analysis program, *J. Appl. Crystallogr.*, 2009, **42**, 339–341.
66 G. M. Sheldrick, Crystal structure refinement with SHELXL, *Acta Crystallogr., Sect. C: Struct. Chem.*, 2015, **71**, 3–8.
67 P. Muller, R. Herbst-Irmer, A. Spek, T. Schneider and M. Sawaya, *Crystal Structure Refinement: A Crystallographer's Guide to SHELXL*, OUP, Oxford, 2006, vol. 8.
68 A. Thorn, B. Dittrich and G. M. Sheldrick, Enhanced rigid-bond restraints, *Acta Crystallogr., Sect. A: Found. Crystallogr.*, 2012, **68**, 448–451.